Journal of Applied Sciences

ISSN 1812-5654

science alert

ANSInet
an open access publisher
http://ansinet.com

Journal of Applied Sciences 11 (15): 2773-2781, 2011
ISSN 1812-5654 / DOI: 10.3923/jas.2011.2773.2781

Non-Dimensional Seismic Charts of Active and Passive Forces in Retaining Walls using Stress Fields

[1]ArashTotonchi and [2]Farajolah Askari
[1]Department of Civil, Marvdasht Branch, Islamic Azad University, Marvdasht, Fars, Islamic Republic of Iran
[2]Iran International Earthquake Engineering Institute, Tehran, Islamic Republic of Iran

Abstract: This study is devoted to find an Analytical solution to investigate the lateral force affection on retaining walls, using mathematical relations based on lower bound limit analysis method. The lower bound of the exact solution can be obtained by use of different admissible stress fields in different regions of the media divided by stress discontinuity surfaces. This process is included the calculation of direction and magnitude of active and passive lateral earth pressure. Numerical results of proposed algorithm are presented in some practical dimensionless graphs.

Key words: Limit analysis, stress discontinuity surfaces, lateral pressure, retaining wall

INTRODUCTION

Mononobe and Matsuo (1929) and Okabe (1926) proposed the well-known Mononobe-Okabe analysis of seismic lateral earth pressure. The analysis is a direct modification of the coulomb wedge analysis. In the analysis, the earthquake effects are replaced by a quasi-static inertia force whose magnitude is computed on the basis of the seismic coefficient concept. As in the coulomb analysis, the failure surface is assumed planer in the Mononobe-Okabe method, regardless of the fact that the most critical sliding surface may be curved. Similar to the coulomb's, the Mononobe-Okabe analysis may underestimate the active earth pressure and overestimate the passive earth pressure. This solution is therefore practically acceptable at least for the active pressure case, although its applicability to the passive pressure is somewhat in doubt.

Some researches were done after Mononobe-Okabe Analysis by Lyamin and Sloan (2002), Chang (2002), Farzaneh and Askari (2003), Bhasin and Kaynia (2004) and Hack *et al.* (2007), to improve this method of analysis. Their studies were included different method of analyzing such as numerical solutions using upper bound and lower bound method of limit analysis theory. As stated in the lower-bound theorem, if an equilibrium state of stress below yield can be found which satisfies the stress boundary conditions, then the loads imposed can be carried without collapse by a stable body composed of elastic-perfectly plastic material (Collins, 2005). Any such field of stress thus gives a safe or lower bound on the collapse or limit load. The stress field satisfying all these conditions is called statically admissible stress field.

In this study, the lower-bound method of limit analysis is applied to include the earthquake effect which is investigated in producing some dimensionless charts for computing the seismic active and passive earth pressure.

THEOREMS OF LIMIT ANALYSIS

Figure 1 shows a typical load-displacement curve as it might be measured for a surface footing test. The curve consists of an elastic portion; a region of transition from mainly elastic to mainly plastic behavior; a plastic region, in which the load increases very little while the deflection increases manifold; and finally, a work-hardening region. In a case such as this, there exists no physical collapse load. However, to know the load at which the footing will deform excessively has obvious practical importance. For this purpose, idealizing the soil as a perfectly plastic medium and neglecting the changes in geometry lead to the condition in which displacements can increase without limit while the load is held constant as shown in Fig. 1. A load computed on the basis of this ideal situation is called plastic limit load (Burland *et al*., 1996). This hypothetical limit load usually gives a good approximation to the physical plastic collapse load or the load at which deformations become excessive. The methods of limit analysis furnish bounding estimates to this hypothetical limit load.

Corresponding Author: ArashTotonchi, Department of Civil, Marvdasht Branch, Islamic Azad University, Marvdasht, Fars, Islamic Republic of Iran

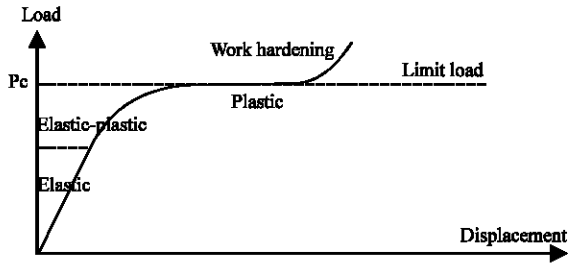

Fig. 1: Load-displacement curve

The theorems of limit analysis can be established directly for a general body if the body possesses the following ideal properties:

- The material exhibits perfect or ideal plasticity, i.e. work hardening or work softening does not occur. This implies that stress point can not move outside the yield surface
- The yield surface is convex and the plastic strain rates are derivable from the yield function through the associated flow rule
- Changes in geometry of the body that occur at the limit load are in significant; hence the equations of virtual work can be applied
- In summary, the limit load is defined as the plastic collapse load of an ideal body having the ideal properties listed above and replacing the actual one

THE LOWER BOUND METHOD

The lower-bound method of limit analysis is different from the upper-bound method in that the equilibrium equation and yield condition instead of the work equation and failure mechanism are considered (Kramer, 1996). Moreover whereas the development of the work equation from an assumed collapse mechanism is always clear, many engineers find the construction of a plastic equilibrium stress field to be quite unrelated to physical intuition. Without physical insight there is trouble in finding effective ways to alter the stress fields when they do not give a close bound on the collapse or limit load. Often the user employs the existing stress fields from well-known texts or the more recent technical literature as a magic handbook and tries to fit his problem to the particular solutions he finds. Intuition and innovation seem discouraged by unfamiliarity and apparent complexity (Zhao *et al*., 2005). Although the discontinuous fields of stress which will be drawn and discussed in this Section are simpler to visualize, they too are not often employed in an original manner by the design engineer (Li *et al*., 2009; Merifield *et al*., 2006). Yet, in fact, the concepts are familiar to the civil engineer in his terms and can be utilized by the designer as a working tool.

The conditions required to establish such a lower-bound solution are essentially as follows:

- A complete stress distribution or stress field must be found, everywhere satisfying the differential equation of equilibrium
- The stress field at the boundary and discontinuities must satisfy the stress boundary conditions
- The stress field must nowhere violate the yield condition

ANALYTICAL SOLUTION FOR ACTIVE CASE

The typical 2D wall geometry for the problem of this study is shown in Fig. 2. Assuming a discontinuity surface, Fig. 2 is showing the variation of stresses in the vicinity of the wall (zone A) and beyond the discontinuity surface (zone B). The final target of the calculations is leading to evaluation of P_{ah} and P_{av} which are the stresses subjected to the earthquake affected on the wall. In this solution the following relation is assumed:

$$\frac{C_w}{C} = \frac{\tan(\Phi_w)}{\tan(\Phi)}$$

where, c and Φ are known as the strength parameters of the material; c represents the cohesion and Φ represents the angle of internal friction. cw is the cohesion and Φw is the internal friction angle between wall and soil. Knowing stresses quantities in element B, the position of S_b is drawn in Fig. 3.

The Mohr circle center and radius are considered as S_a, S_b and r_a, r_b respectively for zones A and B.

The soil is modeled by Mohr-Coulomb yield criterion with various quantities of friction angle and soil cohesion. In a direct application of the Mohr-Coulomb criterion for plane strain stability problems, it is implicitly assumed that the strength of the soil along the failure surface is fully mobilized everywhere along the surface. This is probably the case in most laboratory tests in which the tested specimen is assumed representative of a soil element in the soil mass. This is because the specimen is generally so small that the strain is practically considered uniform along the failure surface, although boundary restrains do exist in almost all tests. For simplicity, the effect of seepage (or pore pressures) on the stability of cohesive-frictional soils has not been included in this study. It is also possible to incorporate the effect of pore pressures in limit analysis but this extension is not being

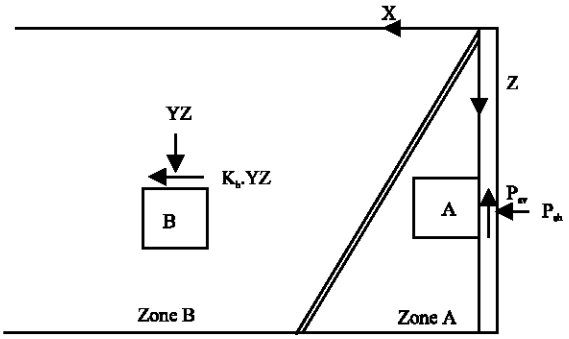

Fig. 2: Stress discontinuity surface, zones A and B

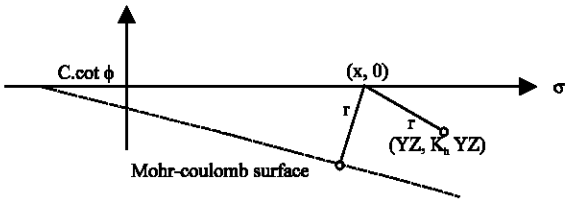

Fig. 3: Assuming S_b as (x, 0)

covered here. The position of stresses of zone B is shown in Fig. 3. The relation of Mohr circle center and radius of zone-B can express by:

$$r = (x+c.\cot\varnothing).\ \sin\varnothing \quad (1)$$

$$r = \sqrt{(\gamma.Z-x)^2 + (K_h.\gamma.Z)^2} \quad (2)$$

Combining Eq. 1 and 2 results in:

$$(x+c.\cot\varnothing)^2\ .\sin^2\varnothing = (\gamma.Z)^2+(x)^2-(2\gamma Z).(x)+(K_h.\gamma Z)^2 \quad (3)$$

Expanding Eq. 3 leads to:

$$(x)^2\ (\sin^2\varnothing-1)+x(2\ c.\cos\varnothing\sin\varnothing+2\gamma Z)+ c^2.\cos^2\varnothing-(K_h.\gamma Z)^2 = 0 \quad (4)$$

where, $x = S_b$. As S_b anr$_b$are calculated, the Mohr circle of zone-B is drawn (Fig. 4).

In Fig. 4 P_b is the pole of Mohr circle of zone-B. For computation of the angle between P_b and the principle surface (α) in Mohr-circle of zone B, using geometrical relations leads to following equations:

$$\tan\alpha = \frac{K_h.\gamma Z}{|\gamma Z - S_b| + r} \quad (5)$$

Substituting r_b in above equation leads to:

$$\alpha = \tan^{-1}\left(\frac{K_h.\gamma Z}{|\gamma Z - S_b| + \sqrt{(\gamma Z - S_b)^2 + (K_h.\gamma Z)^2}}\right) \quad (6)$$

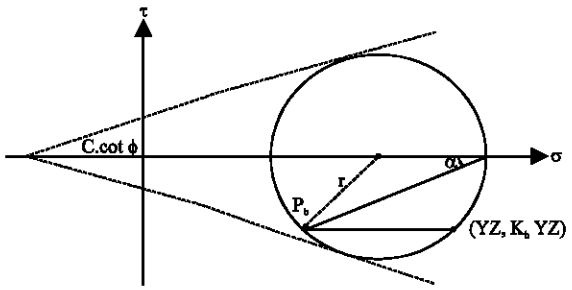

Fig. 4: Mohr circle in zone part B

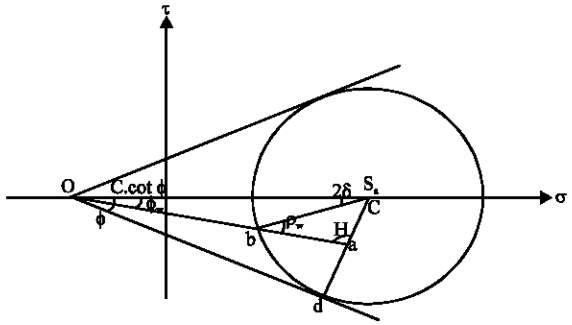

Fig. 5: Assumed Mohr circle in zone part A

Dismounting the wall specifications, the Mohr-circle of zone-A is drawn (Fig. 5). Using Fig. 5 results in the following equations:

$$\frac{\alpha c}{\sin\rho_w} = \frac{bc}{\sin\mu} \quad (7)$$

$$\frac{\alpha c}{\sin\varnothing_w} = \frac{oc}{\sin\mu} \rightarrow \sin\mu = \frac{oc.\sin\varnothing_w}{\alpha c} \quad (8)$$

$$\frac{dc}{\sin\varnothing} = \frac{oc}{\sin 90} \quad \text{and} \quad dc = bc \quad \therefore \quad \frac{bc}{\sin\varnothing} = \frac{oc}{1}$$

$$\sin\varnothing = \frac{bc}{oc} \quad (9)$$

Combining Eq. 4 and 6 results in:

$$\sin\rho_w = \frac{\alpha c}{bc}.\sin\mu \rightarrow \sin\rho_w = \frac{\alpha c}{bc}.\frac{oc}{ac}.\sin\varnothing_w$$

$$\sin\rho_w = \frac{\alpha c}{bc}.\sin\varnothing_w$$

$$\sin\rho_w = \frac{\sin\varnothing_w}{\sin\varnothing} \quad (10)$$

$$\rho_w = 2\delta+\varnothing_w$$

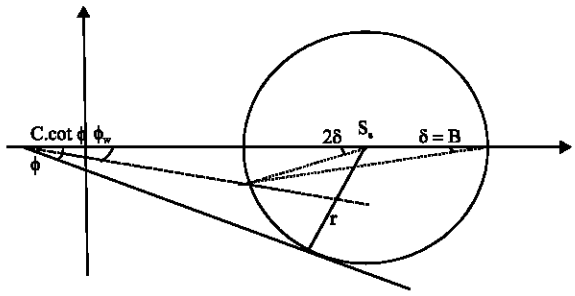

Fig. 6: β recognition

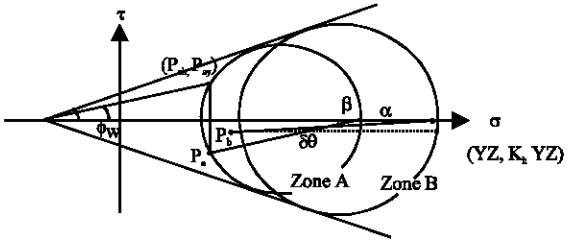

Fig. 7: δθ recognition

$$\delta = \frac{\rho_w - \varnothing_w}{2} \quad (11)$$

Considering β as an angle through zone-A stresses surface and principle surface, the rotation angle of stresses from zone A to B will become to:

$$\beta = \delta = \frac{\rho_w - \varnothing_w}{2} \quad (12)$$

From Fig. 5 and 6, δθ is defined as following equation (Fig. 7):

$$\delta\theta = \beta - \alpha$$

Substituting α and β in above equation leads to:

$$\delta\theta = \frac{\rho_w - \varnothing_w}{2} - \tan^{-1}\left(\frac{K_h.\gamma Z}{|\gamma Z - S_b| + r}\right) \quad (13)$$

In which δθ is rotation angle of stresses from zone B to A. Using the relation between two center point of Mohr-circles of zones A and B, reported by Chen and Liu (1990), the radius Mohr circle of zone A is derived:

$$r_\alpha = (s_\alpha + c.\cot\Phi).\ \mathrm{Sin}\varnothing_{cs} \quad (14)$$

Knowing the quantities of the r_a and S_a, Mohr-circle of element A is drawn. According to Fig. 8, depicting with line throw intersection point of circles (M) and pole B (P_b)

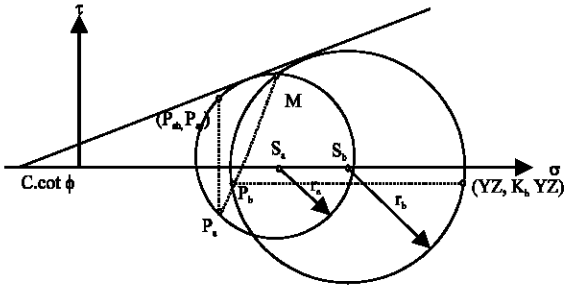

Fig. 8: Calculation results

and extending, pole of Mohr-circle in zone A is appeared which leads to attaining the target.

In summery Calculation algorithm of p_{ah} is defined as follows:

- Calculation of S_b, r_b and α using Eq. 2, 4 and 6
- Calculation of β using Eq. 12
- Determining the rotation angle between the Mohr-circles (δθ = β-α) then use of Eq. 14 and 16 for calculation of S_a and r_a, respectively
- Drawing the Mohr-circles, finding pole of element in zone A which leads to calculation of p_{ah}

Next section is discussed about comparison of this mathematical solution and Mononobe-Okabe Method which results in some tables and graphs.

COMPARISON BETWEEN RESULTS

The Mononobe-Okabe analysis which is an extension of the coulombs analysis, has been experimentally proved by Mononobe-Matsuo to be effective in assessing the seismic active earth pressure. It is generally adopted in the current a seismic design of rigid retaining walls. The Mononobe-Okabe solution is therefore practically acceptable at least for the active pressure case, although its applicability to the passive pressure is somewhat in doubt.

In this section, some results on seismic active pressures as obtained by the present Analytical method are compared with the method of Mononobe-Okabe (M-O) which leads to Table 1 to 4. Comparing the current results with these methods, good agreement is found among them.

In following tables, k_h is horizontal seismic coefficient, δ is friction angle between wall and soil in Mononobe-Okabe method and K_{AE} is active seismic lateral pressure coefficient. For Table 1 to 3 the results are coming out for C = 0, $\Phi_w = \Phi_{cs}/2 = 15°$, H = 5 m, γ = 17.6 kN m^{-3} and for Table 4 which is compared between

Rankin theory and current study, the results are coming out for $\Phi = 30°$, $\gamma = 18$ kN m^{-3}.

So it has been found that the application of limit analysis for cohesionless soil stability problems is practically acceptable. The determination of the seismic lateral earth pressure of a fill on a retaining wall when frictional forces act on the back of the wall, is solved conveniently by this analytical method. As it is seen, the results of Analytical solution and Mononobe-Okabe are practically identical for most cases. By checking out the results of Chung and Chen which are based on upper bound method of limit analysis, it seems that the exact result has a negligible difference with the results of this method.

Table 1: Comparison of K_{AE} for C=0, $\Phi_w = \Phi/2$, $K_h = 0.15$, $K_v = .075$, H = 5 m, $\gamma = 17.6$ kN m^{-3}

	δ	K_{AE}	K_{AE}
Φ	Φ_w	M-O	Analytical Solution
10	5	0.928	0.926
16	8	0.697	0.693
20	10	0.598	0.598
26	13	0.481	0.481
28	14	0.448	0.446
30	15	0.417	0.416
32	16	0.389	0.386
36	18	0.337	0.337
38	19	0.313	0.311
40	20	0.292	0.292

Table 2: Comparison of K_{AE} for C = 0, $\Phi_w = \Phi/2$, H = 5 m, $\gamma = 17.6$ kN m^{-3}

				K_{AE}
Kh	Φ	Φw	M-O	Analytical solution
0.1	30	15	0.373	0.373
0.2	30	15	0.467	0.466
0.3	30	15	0.595	0.595
0.1	10	5	0.795	0.795
0.2	10	5	1.036	1.036
0.3	10	5	0.996	0.996
0.1	40	20	0.257	0.257
0.2	40	20	0.330	0.330
0.3	40	20	0.425	0.425

Table 3: Comparison of K_{AE} for C = 0, $\Phi_w = \Phi_{cs}/2 = 15°$, H = 5 m, $\gamma = 17.6$ kN m^{-3}

K_h	Analytical solution	M-O	Chen and Chung
0.1	0.373	0.373	0.40
0.2	0.466	0.467	0.49
0.3	0.595	0.595	0.62

Table 4: Comparison of active lateral pressure for $\Phi = 30°$, $\gamma = 18$ kN m^{-3}

C(kPa)	Z(Meter)	Rankin	Analytical
10	0	-11.489	-11.489
	10	47.910	47.910
20	0	-22.978	-22.978
	10	36.421	36.421
30	0	-34.467	-34.467
	10	24.932	24.932

NUMERICAL RESULTS FOR ACTIVE CASE

The lower bound solutions obtained can be applied directly in practice and one of the most usable applications of this study is the possibility of introducing some practical dimensionless diagrams for calculating the active seismic lateral force of retaining walls with the considerable accuracy. Figure 9-11 illustrate the active

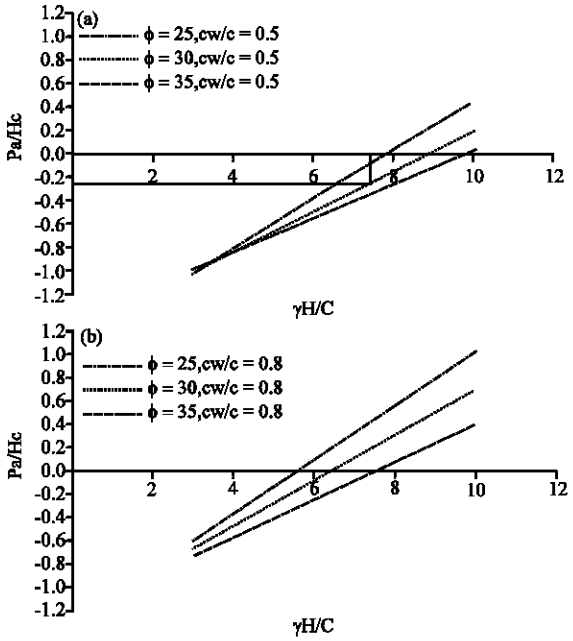

Fig. 9: Dimensionless diagram for calculating the active seismic lateral force, $K_h = 0.1$

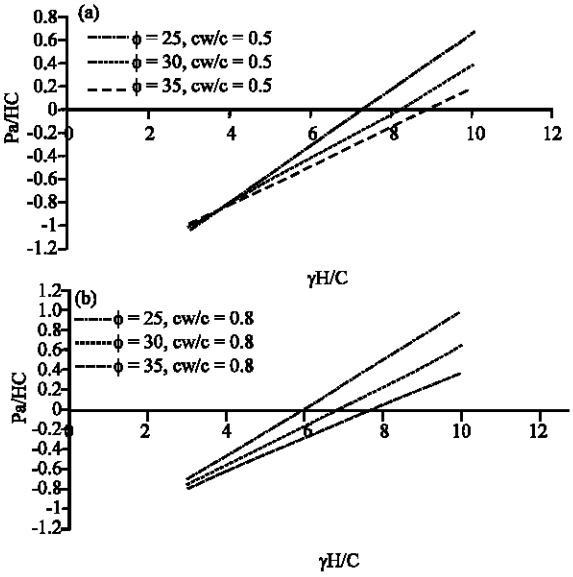

Fig. 10: Dimensionless diagram for calculating the active seismic lateral force, $K_h = 0.2$

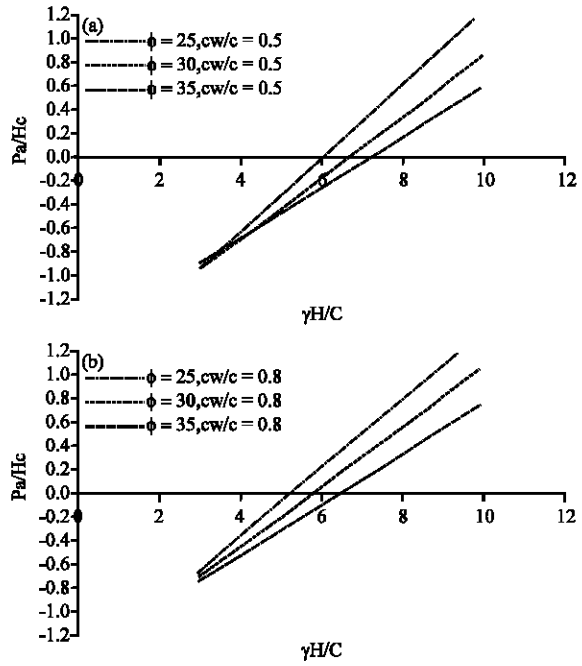

Fig. 11: Dimensionless diagram for calculating the active seismic lateral force, K_h = 0.3

seismic lateral force in various quantities of friction angle and cohesion of the soil and soil-wall. The dimensionless parameters presented are defined as:

$$\lambda = \gamma H/c$$

$$P = Pa/Hc$$

where, γ is soil unit weight, H is the wall height, c is the cohesion of the soil fill back of the wall and P_a is the seismic lateral force which is affected the wall. For each seismic coefficient, the results for three different λ of 3, 5 and 10 are given. To account for the effect of c_w and $\Phi_w$the results are presented in terms of c_w of 0.2, 0.3 and 0.8. As from Fig. 9-11 are displayed, by increasing the soil friction angle, the seismic active force is decreased, as expected. Comparing Fig. 9-11, it seems that for a given λ the active seismic force will increase with increasing c_w/c. Also it seems that increasing in λ and k_h, leads to increase the seismic lateral pressure.

SOLUTION ALGORITHM FOR PASSIVE CASE

Similar to the solution algorithm of active case, using some changes in calculation process the passive seismic lateral earth pressure is computed. Also it can be possible to introduce some practical dimensionless graphs in this case. This algorithm can be able to cover the lack of certainty which lies with Mononobe-Okabe method in passive case. The Mohr-circle of zone-B in passive case is drawn in Fig. 12.

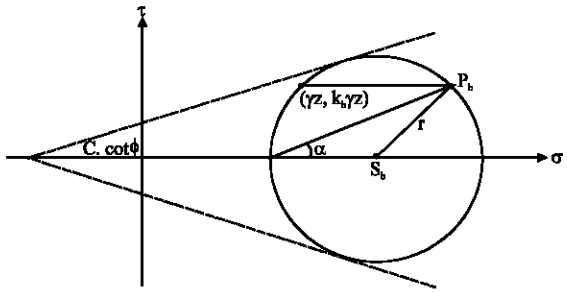

Fig. 12: Mohr-circle of zone-B in passive case

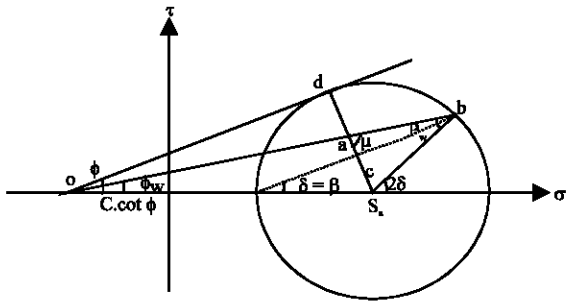

Fig. 13: Assumed Mohr-circle of zone-A

Using geometrical relations leads to following Equations:

$$\tan\alpha = \frac{K_h.\gamma Z}{|\gamma Z - S_b| + r} \quad (15)$$

$$r_b = \sqrt{(\gamma.Z - x)^2 + (K_h.\gamma.Z)^2} \quad (16)$$

Substituting r_b in equation 17 leads to:

$$\alpha = \tan^{-1}\left(\frac{K_h.\gamma Z}{|S_b - \gamma Z| + \sqrt{(\gamma Z - S_b)^2 + (K_h.\gamma Z)^2}}\right) \quad (17)$$

Dismounting the wall specifications, the assumed Mohr-circle of zone-A is drawn (Fig. 13). Using Fig. 13 results in similar equation as active case but β is calculated as follows:

$$\beta = \delta = \frac{\rho_w + \varnothing_w}{2} \quad (18)$$

From Eq. 19 and 20, $\delta\theta$ is defined as following equation (Fig. 14):

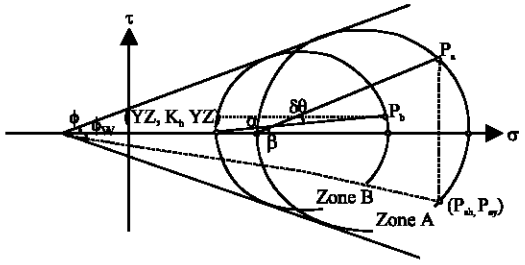

Fig. 14: δθ recognition

$$\delta\theta = \beta - \alpha$$

Substituting α and β in above equation and using the relation between two center point of Mohr-circles of zones A and B, reported by Chen, the Mohr-circle center and radius in zone A are derived.

$$\delta\theta = \frac{\rho_w + \varnothing_w}{2} - \tan^{-1}\left(\frac{K_h.\gamma Z}{|\gamma Z - S_b| + r}\right) \quad (19)$$

$$r_a = (s_a + c.\cot\Phi).\ \mathrm{Sin}\varnothing_{cs} \quad (20)$$

P_{ph} and P_{pv} in Fig. 14 are the horizontal and vertical passive seismic lateral pressure on the wall, respectively.

NUMERICAL RESULTS IN PASSIVE CASE

In this section, some results on static and seismic passive pressures as obtained by the present Analytical method are compared with well-known methods such as Rankin theory (for static case), Ghahramani and Clemence (1980), Chen *et al.* (2003) and modified Dubrova (1963) which leads to Table 5 and 6. Comparing the current results with other methods, good agreement is found among them, so it is concluded that the results of this study is reliable.

As it is seen the result of current solution is close to the other analytical methods and also it can be conservative, therefore the method obtained can be applied directly in practice and one of the most usable applications of this study is the possibility of introducing some practical dimensionless diagrams for calculating the passive seismic lateral pressure coefficient of retaining walls with the considerable accuracy. Fig. 15 to 17 illustrate the passive seismic lateral force in various quantities of friction angle and cohesion of the soil and soil-wall. The dimensionless parameters presented are defined as:

$$\lambda = \gamma H/c$$

$$P = P_p/Hc$$

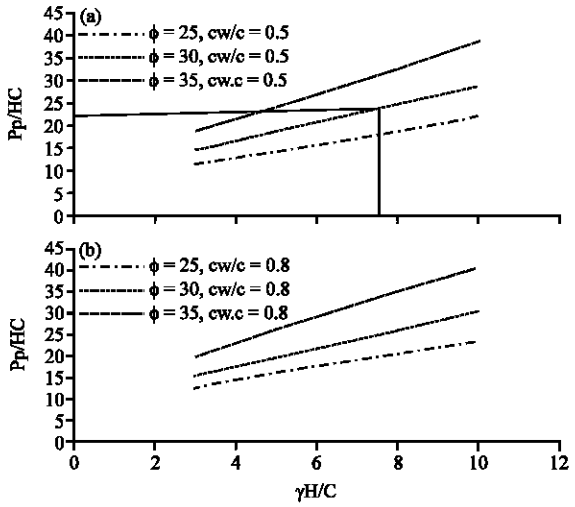

Fig. 15: Dimensionless diagram for calculating the passive seismic lateral force, $K_h = 0.1$

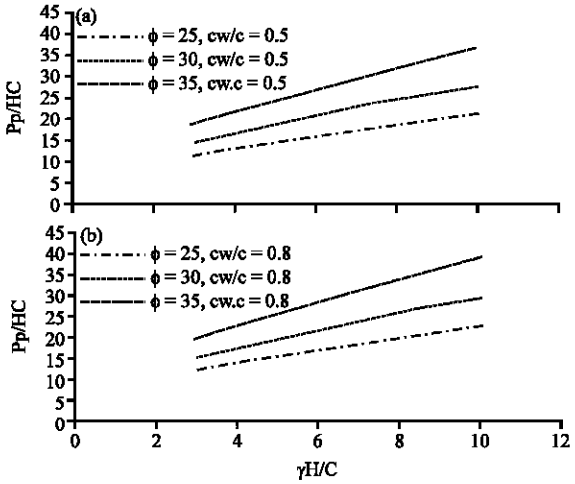

Fig. 16: Dimensionless diagram for calculating the passive seismic lateral force, $K_h = 0.2$

Table 5: Comparison of passive lateral pressure for Φ = 30°, γ = 18 kN m^{-3}, Kh=0

C(kPa)	Z(Meter)	Rankin	Analytical
10	0	34.64	34.64
	10	574.64	574.64
20	0	69.282	69.282
	10	609.282	609.282
30	0	103.923	103.923
	10	643.923	643.923

Table 6: Numerical comparison of solution of various analytical methods for seismic passive earth pressure for vertical wall, ⌀ = 40, $\varnothing_w$ = 2/3⌀, Kh = 0.15

Analytical methods	KPE
Mononobe-Okabe [6]	16.42
Ghahramani-clemence [22]	10.16
Lower bound (current study)	10.16
Upper bound (Chen) [4]	11.88
Modified Dubrova method [23]	16.43

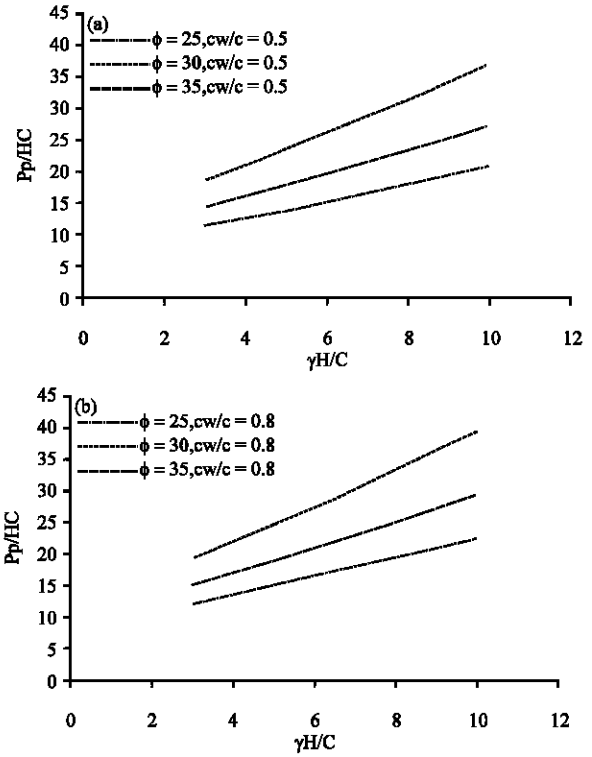

Fig. 17: Dimensionless diagram for calculating the passive seismic lateral force, $K_h = 0.3$

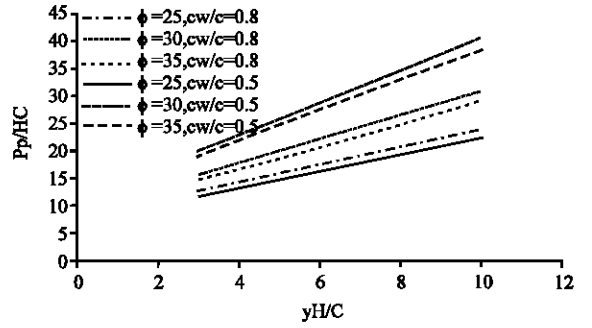

Fig. 18: Results comparison for distinguishing the effect of c_w/c

where, P_p is the passive seismic lateral force which is affected on the wall. For each seismic coefficient, the results for three different λ of 3, 5 and 10 are given. To account for the effect of c_w and $\Phi_w$the results are presented in terms of c_w of 0.2, 0.3 and 0.8. Having found these parameters for each problem, one can compute the conservative seismic passive lateral force in a retaining wall.

As from Fig. 15 to 17 are displayed, by increasing the soil friction angle, the seismic passive force is increased. Fig. 18 is a comparison between the results for

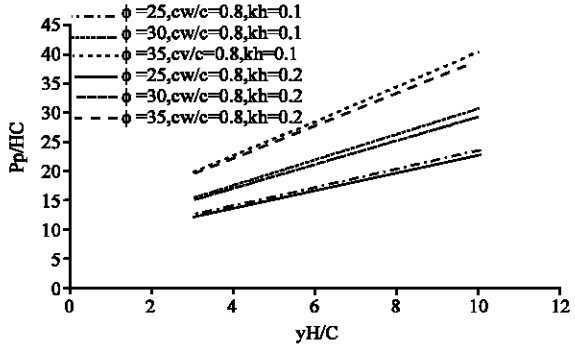

Fig. 19: Results comparison for the effect of k_h

distinguishing the effect of c_w/c; it seems that for a given λ the passive seismic force will increase with increasing c_w/c.

Also from Fig. 19 it seems that increasing in λ leads to increase and increasing in k_h comes to decrease the seismic lateral force (P_p).

EXAMPLE OF APPLICATION

Now it is illustrated how the results in Fig. 9 to 11 and Fig. 15 to 17 can be used to determine the seismic active and passive lateral force.

Problem. A wall is built back of a soil which has following parameters, the height of the wall H = 5 m, the soil unit weight is γ = 15 kN m^{-3}, the soil's strength parameters c = 10kN m^{-2}, Φ = 30 and the soil-wall cohesion c_w = 5 kN m^{-2}. For a seismic coefficient of k_h = 0.1 what is the amount of seismic active and passive lateral force?

A procedure for using the results of the presented study to solve the forgoing problem can be summarized as follows. First active case:

- From the value of γ, H and c, the dimensionless parameter $\lambda = \gamma H/c = 7.5$ is calculated
- With $k_h = 0.1$ and $c_w/c = 0.5$, it follows that the results presented in Fig. 9a should be used to determine the force
- In Fig. 9a, a straight-vertical line passing through $\lambda = 7.5$ is drawn. This straight line will intersect with three curves which the intersection point of curve with $\Phi = 30$ and $c_w/c = 0.5$ is selected
- From this intersection point, it can back-figure the following dimensionless parameter P' from which the lower bound solution of the seismic active force can be calculated as P= -11.23 kN m^{-1}
- Going on the process for passive case, Fig. 15a is chosen and the lower bound solution of the seismic passive force can be calculated as P = 1043.15 kN m^{-1}

CONCLUSION

The active and passive seismic lateral pressures on retaining walls are investigated in this paper. An analytical solution is introduced based on lower bound limit analysis method and solution is compared to the well-known methods such as Mononobe- Okabe, Chung and Chen, Ghahramani-clemence, Dubrova and Rankin which good agreement is found among them. Some practical dimensionless diagrams for calculating the active and passive seismic forces on retaining walls with the considerable accuracy are presented. The results show that in active case by increasing the soil friction angle, the seismic active force is decreased, as expected but in passive case inversely, the seismic passive force is increased. Comparing diagrams, it seems that for a given $\lambda = \gamma H/c$ both active and passive seismic force will increase with increasing c_w/c. Also it is found that increasing in λ leads to increase both active and passive seismic lateral force. Comparing diagrams for various quantities of k_h, shows that increasing in k_h leads to increase the active pressure but the passive pressure decreases.

NOMENCLATURES

c = Cohesion
c_w = Cohesion between soil and wall
Φ = Internal friction angle
Φ_w = Internal friction angle between soil and wall
γ = Soil unit weight
z = Height
P_{pv} = Vertical passive seismic lateral pressure
P_{ph} = Horizontal passive seismic lateral pressure
S_a = Center point of Mohr-circle in zone A
S_b = Center point of Mohr-circle in zone B
r_a = Radius of Mohr-circle in zone A
r_b = Radius of Mohr-circle in zone B
P_a = Pole of zone-A
P_b = Pole of zone-B
α = Angle between P_b and the principle surface
β = Angle between P_a and the principle surface
$\delta\theta$ = Rotation angle of stresses from zone B to A
M = Intersection of Mohr-circles
K_h = Seismic coefficient
λ = Dimensionless parameter = $\gamma H/c$
P_a = Seismic active lateral force
P_p = Seismic passive lateral force
p' = Dimensionless parameter

REFERENCES

Bhasin, R. and A.M. Kaynia, 2004. Static and dynamic simulation of a 700-m high rock slope in western Norway. Eng. Geol., 71: 213-226.

Burland, J.B., S. Rampello, V.N. Georgiannou and G. Calabresi, 1996. A laboratory study of the strength of four stiff clays. Geotechnique, 46: 491-514.

Chang, M., 2002. A 3D slope stability analysis method assuming parallel lines of intersection and differential straining of block contacts. Can. Geotech. J., 39: 799-811.

Chen, J., J.H. Yin and C.F. Lee, 2003. Upper bound limit analysis of slope stability using rigid finite elements and nonlinear programming. Can. Geotech. J., 40: 742-752.

Chen, W.F. and X.L. Liu, 1990. Limit Analysis in Soil Mechanics. Elsevier Publisher, Amsterdam.

Collins, I.F., 2005. Elastic/plastic models for soils and sands. Int. J. Mech. Sci., 47: 493-508.

Dubrova, G.A., 1963. Interaction of Soil and Structures. Rehnoy Transport Publishing, Moscow, USSR.

Farzaneh, O. and F. Askari, 2003. Three-dimensional analysis of nonhomogeneous slopes. J. Geotech. Geoenviron. Eng., 129: 137-145.

Ghahramani, A. and S.P. Clemence, 1980. Zero extension line theory of dynamic passive pressure. J. Geotech. Eng. Div., 106: 631-644.

Hack, R., D. Alkema, G.A.M. Kruse, N. Leenders and L. Luzi, 2007. Influence of earthquakes on the stability of slopes. Eng. Geol., 91: 4-15.

Kramer, S.L., 1996. Geotechnical Earthquake Engineering. 1st Edn., Prentice Hall, New Jersey, ISBN-13: 9780133749434, pp: 653.

Li, A.J., A.V. Lyamin and R.S. Merifield, 2009. Seismic rock slope stability charts based on limit analysis methods. Comput. Geotech., 36: 135-148.

Lyamin, A.V. and S.W. Sloan, 2002. Lower bound limit analysis using non-linear programming. Int. J. Numer. Meth. Eng., 55: 573-611.

Merifield, R.S., A.V. Lyamin and S.W. Sloan, 2006. Limit analysis solutions for the bearing capacity of rock masses using the generalized Hoek-Brown criterion. Int. J. Rock Mech. Mining Sci., 43: 920-937.

Mononobe, N. and H. Matsuo, 1929. On the determination of earth pressure during the earthquake. Proc. World Eng. Conf., 9: 177-185.

Okabe, S., 1926. General theory of earth pressure and seismic stability of retaining wall and dam. J. Jpn. Soc. Civ. Eng., 10: 1277-1323.

Zhao, J., D. Sheng and W. Zhou, 2005. Shear banding analysis of geomaterials by strain gradient enhanced damage model. Int. J. Solids Structure, 42: 5335-5355.